Research Square

Preprints are preliminary reports that have not undergone peer review.
They should not be considered conclusive, used to inform clinical practice,
or referenced by the media as validated information.

An Integrated Framework for the Hydraulic Design and Optimization of In-Ground Stilling Basins

Ebi Meshkati
Boskalis (Netherlands)
Hossein Sohrabzadeh Anzani
sohrabzadeh.hossein.4f@kyoto-u.ac.jp
Disaster Prevention Research Institute, Kyoto University
Binh Quang Nguyen
University of Da Nang
Sameh Ahmed Kantoush
Disaster Prevention Research Institute, Kyoto University
Tetsuya Sumi
Disaster Prevention Research Institute, Kyoto University

Research Article

Keywords: In-Ground Stilling Basins (ISB), Hydraulic Jump, Energy Dissipation, Experimental Hydraulics, Geometric Optimization

Posted Date: November 12th, 2026

DOI: https://doi.org/10.21203/rs.3.rs-11548950/v1

License: This work is licensed under a Creative Commons Attribution 4.0 International License.
Read Full License

Additional Declarations: No competing interests reported.

An Integrated Framework for the Hydraulic Design and Optimization of In-Ground Stilling Basins

Abstract

The flow exiting a dam's bottom outlet typically forms a supercritical jet. Upon encountering a hydraulic jump, the supercritical jet transitions rapidly into subcritical flow, effectively dissipating energy. To mitigate potential damage, such as structural failure or downstream scour, a stilling basin is commonly used for energy dissipation. Existing literature identifies several energy dissipation mechanisms in stilling basins, including abrupt drops, sudden enlargements, positive steps, and cross-walls. However, the combined effects of these parameters have not been extensively explored. This study aims to develop an analytical model for optimizing the geometry of the In-Ground Stilling Basin (ISB) and improving energy dissipation. To address this research gap, extensive experimental analyses were performed at the Ujigawa Open Hydraulic Laboratory, Disaster Prevention Research Institute (DPRI), Kyoto University, Japan. Experimental results indicate that ISB geometry directly influences flow patterns and basin performance. It is necessary to identify the relevant flow pattern and propose a design guideline for that specific pattern. Therefore, the author provided a step-by-step design procedure for the ISB's downstream. In addition, empirical and theoretical equations were formulated to predict energy loss and sequent depth, demonstrating strong agreement with the experimental data in the complex ISB geometry.

Keywords: In-Ground Stilling Basins (ISB), Hydraulic Jump, Energy Dissipation, Experimental Hydraulics, Geometric Optimization.

Highlights:

– Identified Steady Submerged Jump (SSJ) as the most efficient ISB flow, maximizing energy dissipation and symmetry.

– Proposed a comprehensive design procedure integrating drop, expansion, and end-sill effects in ISBs.

– Formulated and validated new empirical equations for key ISB parameters using 110 experiments.

– Developed universal flow maps with non-dimensional parameters for quick ISB design and assessment.

1. INTRODUCTION

Dams are essential infrastructure in mitigating flood risks, especially Flood Mitigation Dams (FMDs), known internationally as 'dry dams', designed explicitly to attenuate flood peaks (Kantoush and Sumi, 2010). These gateless bottom outlet structures regulate flood peaks by controlling flow discharge, ensuring that downstream river capacity is not exceeded during flood events (Sumi, 2008). Excess flow is directed into the downstream river through the bottom outlet (Meshkati et al., 2013). However, the high velocity and energy of this discharge can pose significant risks to both the downstream infrastructure and the dam itself if proper energy dissipation measures are not implemented (Akan, 2010). To mitigate this, specialized energy dissipation structures are integrated into dam designs. Among these, stilling basins (SBs) play a crucial role in reducing flow energy, primarily through hydraulic jumps or turbulent flow mechanisms, thereby preventing structural damage to the dam and its surroundings (Kiani et al., 2017) (Fig. 1).

A hydraulic jump is a phenomenon characterized by a rapid change in flow conditions, transitioning from supercritical to subcritical flow, with a substantial dissipation of energy (Hager, 1992). These jumps commonly occur at the toe of a weir or where a sloped channel abruptly flattens (Chow, 1959), where supercritical flow encounters an abrupt reduction in channel slope. The jump happens when supercritical flow is forced to transition into subcritical flow (Mahtabi et al., 2020). The nature of the

hydraulic jump, whether submerged or unsubmerged, depends on the tailwater conditions downstream (Bremen, 1990).

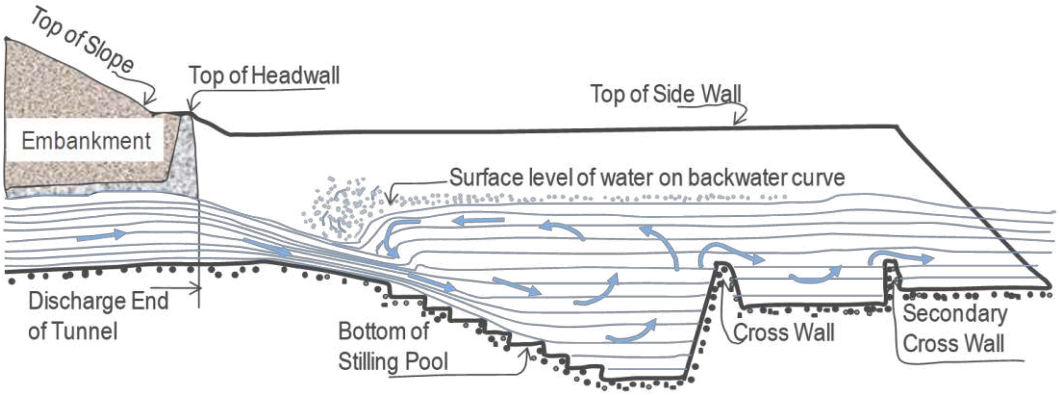


Fig. 1. Conceptual schematic view of an in-ground stilling basin, Taylorsville FMD, constructed by Miami Conservation District, USA.

Stilling basins worldwide share a common objective: to dissipate flow energy efficiently and cost-effectively. However, their configurations vary significantly depending on the specific requirements of their applications. For example, a stilling basin designed for high-level outlets, such as spillways, may not be suitable for low-level outlets, such as culverts, due to the distinct hydraulic conditions governing each application. This study examines stilling basins situated downstream of FMDs, commonly referred to as "dry dams" in the United States (Kantoush and Sumi, 2010). An FMD is a gateless structure with a low-level bottom outlet designed to attenuate flood peaks, ensuring that downstream discharge remains within the river channel's capacity during various flood events (Sumi, 2008). Generally, the bottom outlet of an FMD is centrally positioned at the dam base, causing symmetrical sudden expansions in the downstream stilling basin. The expansion ratio, defined as $k = b_1/B_r$, where b_1 is the outlet width and B_r is the downstream river width, is generally small, ranging from 0.15 to 0.3. However, these small expansion ratios are unfavourable for design purposes as they often lead to significant flow instability and periodicity within the stilling basin (Ohtsu et al., 1999). To mitigate these effects, structural modifications such as abrupt drops, cross-walls, and baffles are employed to stabilize the flow. This study focuses on the performance of an "in-ground" stilling basin (ISB), which resembles a box-like pool situated below the FMD outlet. A typical ISB design includes a sudden expansion combined with an abrupt drop at the upstream end, followed by a positive step and cross walls downstream.

78 The impact of design modifications, such as abrupt drops, sudden expansions, and cross-walls, on
79 flow characteristics within conventional stilling basins has been extensively studied (e.g., Rajaratnam
80 and Subramanya, 1968; Ohtsu and Yasuda, 1991; Bremen and Hager, 1994; Negm, 2003). Ohtsu and
81 Yasuda (1991) classified abrupt drops based on the drop number (s/h_1, where s is the drop height and h_1
82 is the outlet opening height) into three categories: low, medium, and high. In their classification, drop
83 numbers ranging from $0.5 \leq s/h_1 \leq 8-9$ were considered low drops. They observed that regardless of the
84 drop classification, the flow characteristics downstream of a drop are influenced by the approaching
85 Froude number (F_1). The three-dimensional flow patterns below abrupt drops have been
86 comprehensively discussed by researchers such as Ohtsu and Yasuda (1991), and Pagliara (1992), with
87 Ferreri and Nassello (2002) summarizing these findings. Hager and Bremen (1992) classified the flow
88 behaviour downstream of a sudden expansion into four main types, depending on inflow conditions:
89 reattachment jump (R-jump), spatial jump, transitional jump, and classical hydraulic jump. They
90 concluded that, despite their practical applications, sudden expansions alone are not effective in
91 dissipating flow energy. Additionally, Ohtsu et al. (1999) investigated submerged hydraulic jumps
92 downstream of sudden expansions, categorizing them into three types: asymmetric submerged jump
93 (ASJ), periodic submerged jump (PSJ), and steady submerged jump (SSJ). They recommended SSJ as
94 the most desirable flow pattern due to its stability and symmetry.
95 Ohtsu et al. (1999) further highlighted that the flow patterns within a stilling basin are primarily
96 governed by geometrical parameters, such as the expansion ratio, rather than the inflow Froude number
97 (F_1). However, while their study encompassed a broad range of experimental conditions, it did not
98 address the influence of drop numbers or cross-wall heights on energy dissipation within the stilling
99 basin. Zare and Doering (2011) studied forced submerged hydraulic jumps in both prismatic and non-
100 prismatic stilling basins. Expanding on the work of Ohtsu et al. (1999), they proposed an equation to
101 estimate the required stilling basin length under these conditions. Their results showed that incorporating
102 sills within the basin reduced the required length compared to the estimates provided by Ohtsu et al.
103 (1999). However, the stilling basin geometries analyzed by Zare and Doering (2011) did not include key
104 design features such as drops or cross-walls, which are commonly employed to improve flow
105 stabilization and enhance energy dissipation. Katakam and Rama (1988) investigated the combined

effects of an abrupt drop and a sudden expansion on flow behaviour. They derived a three-dimensional expression by incorporating both the expansion ratio and the drop number into the momentum equation to estimate the sequent depth ratio (Y_2) downstream. Their findings indicated that the simultaneous occurrence of a sudden expansion and an abrupt drop can create a new flow pattern, referred to as the Special B-jump. This flow pattern, as reported in their study, requires a lower sequent depth ratio to form and demonstrates greater stability and enhanced energy dissipation compared to either an abrupt drop or a sudden expansion.

Most existing studies have focused primarily on the flow characteristics within stilling basins, often overlooking the flow dynamics downstream. Larson (2004) made a significant contribution by considering both the flow behaviour inside and downstream of the stilling basin. Her study examined the effect of a cross-wall on the energy dissipation process in a culvert. In determining the optimal cross-wall height, Larson not only addressed the stability and energy dissipation of the flow but also considered the velocity just downstream of the cross-wall, where free-fall conditions could lead to significant erosion. However, the geometry in Larson's study did not incorporate a sudden expansion upstream. To date, no comprehensive study has investigated the combined effects of an abrupt drop, sudden expansion, positive step, and cross wall on flow patterns and energy dissipation within a stilling basin. In particular, the behaviour of forced submerged hydraulic jumps within such a complex configuration remains unexamined. This knowledge gap motivates the present experimental study, which explores the influence of five key geometric and hydraulic variables: Froude number, ISB depth, ISB length, cross-wall height, and cross-wall width. The primary objectives of this study are: (i) to identify the critical non-dimensional parameters governing flow behaviour under forced submerged hydraulic jumps, (ii) to develop an analytical model for optimizing ISB geometry and energy dissipation, and (iii) to propose an empirical method for adjusting cross-wall height based on downstream flow requirements.

2. LABORATORY SETUP AND TESTING APPROACH

2.1. Physical model design

The experimental investigation was conducted at the Ujigawa Open Hydraulic Laboratory, Disaster Prevention Research Institute (DPRI), Kyoto University, Japan. A precision-engineered horizontal

rectangular flume with 0.2 mm level bed tolerance verified by laser, measuring 11 m in length, 0.5 m in width, and 0.5 m in height, was utilized for the study. The flume's base was constructed from a metal sheet to ensure structural stability, while its sidewalls were fabricated from laminated glass to facilitate clear visualization of flow dynamics during testing.

The physical model's dimensions were precisely scaled to reflect typical geometric features derived from three representative Japanese FMDs: Masudagawa, Tsuzuki, and Mogamioguni. A geometric length scale ratio of 1:40 was adopted, ensuring appropriate scaling of the physical system. Dynamic similarity between the prototype and scaled models was ensured by maintaining consistent Froude numbers, adhering to the principles of Froude similarity by maintaining identical Froude numbers between the prototype and scaled experiments, the scale ratio for velocities, discharges, and other relevant hydraulic parameters was determined.

In the prototype FMDs, a 100-year return period flood event typically generates flow conditions characterized by Froude numbers ranging from 3 to 6 at the bottom outlet. By replicating these hydraulic conditions, the physical model effectively preserved the influence of inertial and gravitational forces, thereby enabling a robust and scalable analysis of flow behaviour and energy dissipation mechanisms within the stilling basin. The experimental program examined the effects of approach Froude number, basin drop depth, basin length, and end-sill height on flow characteristics. The physical-model dimensions are summarized in Table 1, and the distribution of experimental cases among flow regimes is presented in Table 2.

Table 1 provides a comprehensive summary of the tested ISB configurations, highlighting variations in key parameters. The experiments included three different ISB lengths (75 cm, 100 cm, and 125 cm) and step depths s of 5 cm, 10 cm, and 15 cm. For each ISB configuration, end-sills of varying heights (h_e = 0, 4, 8, 12, and 13.5 cm) were systematically analyzed to identify the optimal design. These end-sills were positioned vertically above the positive step and oriented perpendicularly to the flume's longitudinal axis. The investigation also explored the effect of the end-sill width, with free space on either side (b_e) set to 50 cm, 40 cm, 30 cm, and 20 cm. Additionally, three different Froude numbers (Fr_1 = 2.8, 4.9, and 5.1) of the supercritical flow at the bottom outlet were examined. The bottom outlet geometry was kept constant, with a height (h_1) of 5 cm and a width (b_1) of 10 cm, resulting in an

expansion ratio ($k = b_1/B$) of 0.2. This expansion ratio aligns closely with the average practical values for FMDs.

Table 1. Dimensions of the physical model used in the present study.

Item	Prototype	Physical model	Factor of Scale
ISB length [m]	26 – 56	0.65 – 1.40	40
ISB width [m]	20	0.50	40
Drop height [m]	1 – 4	0.025 – 0.100	40
Bottom outlet height [m]	1.9 – 3.4	0.0475 – 0.085	40
Bottom outlet width [m]	1.7 – 4.45	0.0425 – 0.111	40
Discharge [m^3s^{-1}]	40 – 320	0.0039 – 0.031	40

The physical model of the ISBs was designed to allow systematic adjustments to its geometry, such as depth and length, by integrating precisely crafted wooden components securely adhered to the model structure. Water recirculation during the experiments was maintained using a centrifugal pump connected to a closed-loop piping system. Flow discharge was accurately controlled using a calibrated 90-degree V-notch weir positioned upstream of the experimental setup.

Water depth fluctuations along the ISB were monitored using an electromagnetic water level meter (manufactured by JFE Advantech, Japan). Measurements were taken at three critical cross-sections: the dam outlet face, the cross-wall, and downstream of the cross-wall. At each cross-section, water depths were recorded at four distinct points, and the average value was used for data analysis. The measurements were conducted with a sampling frequency of 50 Hz, with approximately 32,000 samples collected per point. The characteristics of the hydraulic jump were comprehensively documented through visual observation, high-resolution photography, and video recordings from both top and side views, facilitated by the transparent Plexiglas sidewalls of the flume. Furthermore, surface velocity fields were measured using a large-scale particle image velocimetry (LSPIV) system, while three-dimensional velocity profiles were obtained through an ultrasonic Doppler velocity profiler (UVP). These measurement techniques provided detailed insights into the flow dynamics and behavior within the ISB. The transparent Plexiglas sidewalls of the flume provided unobstructed visibility, enabling

precise documentation of the flow behavior.

2.2. Experimental conditions and dimensional analysis

The hydraulic performance (*HP*) of ISB depends on the following parameters (Meshkati et al., 2025):

$$HP = f(U_o, b_1, h_1, h_2, h_3, s, B, L, h_e, Q, \rho, g, \sigma, \mu) \quad (1)$$

where U_o is the outlet velocity at the bottom outlet face, b_1 is the bottom outlet width, h_1 is the bottom outlet height, s is the drop height, B is the ISB width, L is the ISB length, h_2 *is* the sequent depth, h_e is the cross wall height, Q is discharge, ρ is the water density, σ is the surface tension, μ is the dynamic viscosity of water, and g is the gravitational acceleration.

Using dimensional analysis, the parameters in Eq. 1 reduce to Eq. 2:

$$HP = f\left(Y_2, Y_3, \frac{s}{h_1}, \frac{L}{B}, K, a, \frac{h_1}{B}, \frac{h_e}{h_c}, \mathrm{W}, \mathrm{Re}, \mathrm{Fr}_1\right) \quad (2)$$

Here $\mathrm{W}=\frac{\rho L U_o^2}{\sigma}$, $\mathrm{Re}=\frac{\rho U_o h_1}{\mu}$, and $\mathrm{Fr}=\frac{U_o}{(g h_1)^{0.5}}$ are Weber, Reynolds, and Froude numbers, respectively. These numbers are commonly used in the study of fluid dynamics (Sohrabzadeh and Ghodsian, 2023, and 2024; Sangsefidi et al., 2020; Sohrabzadeh et al., 2024 a, b; Anzani et al., 2025a and b). In the dimensional analysis, the parameter of Y_2 denotes the normalized sequent depth (ratio of sequent depth to outlet height, h_2/h_1), and Y_3 represents the degree of submergence (ratio of downstream depth to outlet height, h_3/h_1), K is the expansion ratio (b_1/B), a is the outlet aspect ratio (h_1/b_1), and h_c is the critical depth $(Q^2/(gB^2)^{\frac{1}{3}})$. Also, L/B is the ISB aspect ratio, s/h_1 is the drop number, and h_e/h_c is the normalized cross-wall height.

The dimensions of the bottom outlet (h_1 = 5 cm and b_1 = 10 cm) and the width of the ISB (B = 50 cm) were constant. The fixed outlet dimensions imply a constant expansion ratio ($K = b_1/B$) of 0.2 and a given outlet aspect ratio ($a = h_1/b_1$) of 0.5, which are both commonly used by engineers in commercial/field scale.

Kiani et al. (2017) showed that viscous effects were deemed negligible for Reynolds numbers (Re) greater than 10000. Following Heller (2011), surface tension effects can be neglected in the analysis as the square root of the Weber number exceeds 110 for all the tests in this study, allowing us to omit the

surface tension from Eq. 2. Therefore, the normalized hydraulic performance (*NHP*) of ISB can then be written as follows:

$$NHP = f\left(Y_2, Y_3, \frac{s}{h_1}, \frac{L}{B}, \frac{h_e}{h_c}, \mathrm{Fr}_1\right) \quad (3)$$

Table 2 summarizes the non-dimensional parameters used in the test runs conducted in this study.

Table 2. Non-dimensional test parameters.

Fr_1	L/B	s/h_1	h_e/h_c	Y_2	Y_3	Jump types	No. Exp.
2.85 – 4.99	1.5, 2, 2.5	1, 2, 3	0 – 0.75	2.17 – 5.28	0.25 – 1.18	BJ	25
2.85 – 4.99	1.5, 2, 2.5	1, 2, 3	0.75 – 2.66	2.99 – 6.10	1.05 – 3.22	UJ	27
2.85 – 4.99	1.5, 2, 2.5	1, 2, 3	1.50 – 3.52	3.83 – 6.94	2.21 – 3.64	PSJ	21
2.85 – 4.99	1.5, 2, 2.5	1, 2, 3	1.50 – 3.97	4.71 – 7.09	2.41 – 3.92	SSJ	37
			Total No. Exp.				110

3. RESULTS AND DISCUSSION

3.1. Selection of optimum geometry of stilling basin

The experimental outcomes indicate that within the Froude number range of 2.5–5.5, the performance of the ISB predominantly depends on its geometric configuration rather than upstream hydraulic conditions. The main geometric parameters of an ISB include ISB length, ISB depth, end-sill height, and the width of the end-sill. For a Froude number range of 2.5 to 5.5, and an expansion ratio of 0.2 (k = 0.2), the optimum selected cases of ISB geometry should satisfy the following geometrical parameters: $2 < h_e/h_c < 3$, $L/B = 2$, $s/h_1 = 2$, and $1 - (b_e/B) = 0.2$ (Fig. 2).

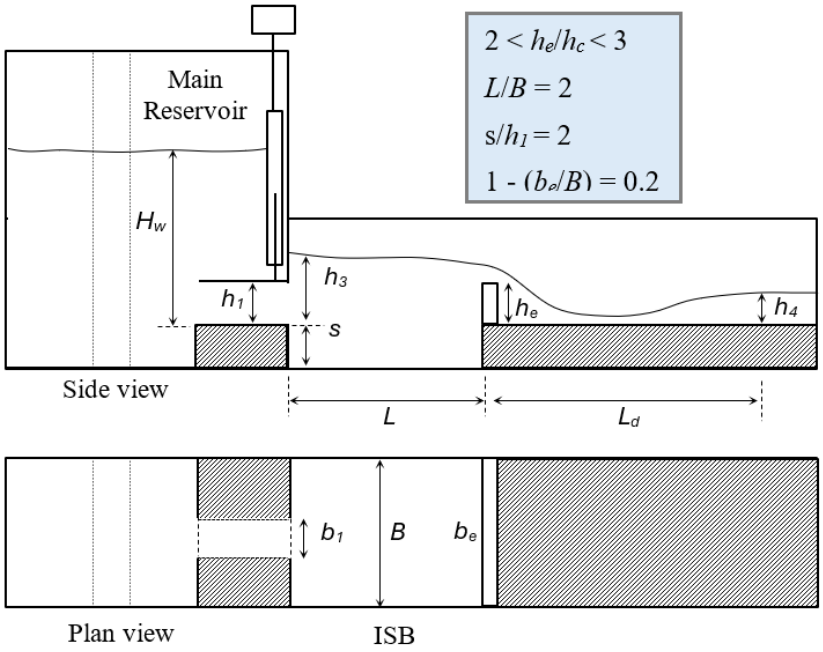
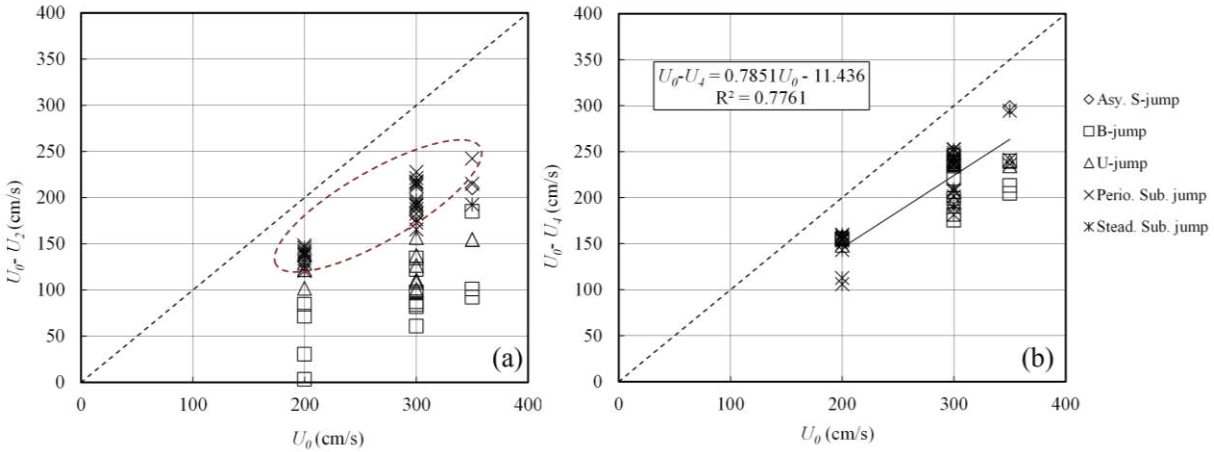


Fig. 2. The optimum selected cases of ISB geometry should satisfy the following geometric parameters.

3.2. Target flow pattern

Figure 3a depicts the velocity reduction along and within the ISB for the ISB configurations represented in the experimental dataset. The horizontal axis is the initial velocity at the face of the bottom outlet, U_0, and the vertical axis measures the change in maximum velocity between sections I and II. All five different flow patterns, B-jump, asymmetric S-jump, U-jump, periodic submerged jump, and steady submerged jump, were plotted in this graph. The figure revealed that the largest velocity reduction (U_0 - U_2) along the centerline and within the ISB is provided by the periodic and steady submerged jumps, while asymmetric S-jump and B-jumps show much less in terms of velocity reduction. Figure 3b is a flow pattern map based on velocity reduction between section I (at the face of the bottom outlet) and section IV (downstream of ISB).



233

234 **Fig. 3.** Flow pattern map for 65 different geometries, velocity reduction between (a) sections I and II,
235 (b) sections I and IV.

236 It can be interpreted that downstream of the ISB, there is no significant difference in velocity
237 reduction between the five possible flow patterns. However, the submerged hydraulic jumps still provide
238 a greater reduction in velocity between sections *I* and *IV*. To conclude, for the purpose of optimizing
239 ISB design guidelines, steady submerged hydraulic jumps were identified as the most favorable due to
240 their superior performance in energy dissipation and downstream flow stabilization.

241 **3.3. Target windows for ISB geometries**

242 Figure 4a illustrates the universal flow pattern map. This flow pattern map is based on normalized
243 parameters, and it consists of both geometric and hydraulic parameters. This universal flow pattern map
244 can be used for the first estimation of ISB geometries in design. Moreover, it can be utilized to check
245 whether the designed geometry of ISB can provide us with a desirable flow pattern or not. Herein, using
246 this flow pattern map, a target window for the acceptable geometry of an ISB is introduced.

247

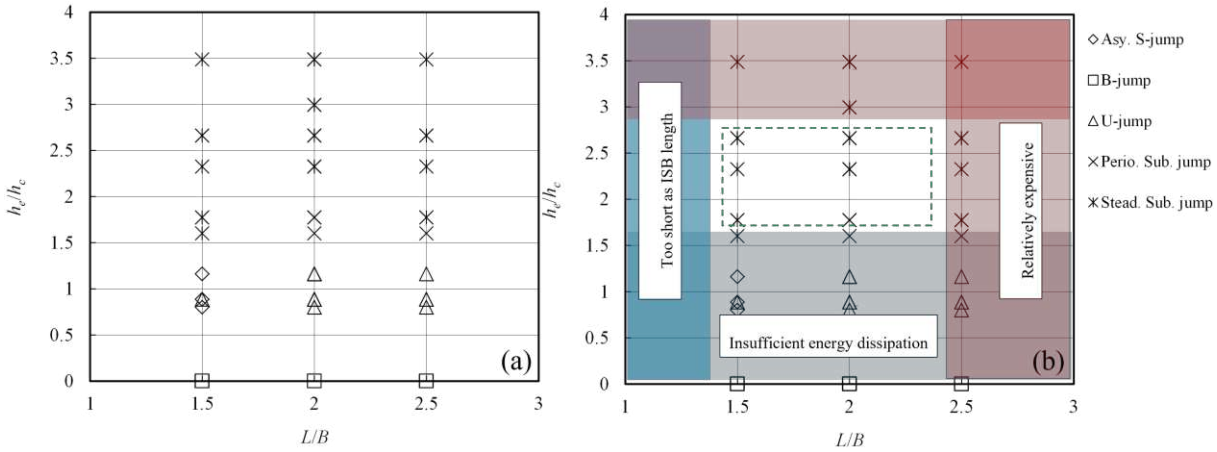


Fig. 4. (a) Universal flow pattern map, relative end-sill height versus relative stilling basin length. (b) Acceptable window in flow pattern map for design purposes, considering the aspect ratio and normalized end-sill height.

To define the acceptable geometry of an ISB, both hydraulic and economic criteria should be considered. S-jump, B-jump, and U-jump are characterized by an upward plunging jet and high velocity at the water surface. These types of jumps generally cannot sufficiently dissipate the energy of the outflow from the FMD's bottom outlet. In Figure 4b, the flow pattern map from Figure 4a has been colored and annotated to highlight the various regions of significance. An ISB where the relative end-sill height is less than 1.5 cannot produce sufficient energy dissipation, regardless of the Froude number or normalized ISB length. This area is therefore highlighted in blue to indicate that it is not recommended for design.

Considering the economic aspects, a normalized end-sill height, h_e/h_c, greater than 3 (red region in Figure 4b) may not be cost-efficient; thus, it is suggested to avoid such a design. Also, normalized ISB lengths, L/B, greater than 2.5 and less than 1.5 may not be suitable. A longer ISB length is too expensive, and a shorter length may not be able to provide enough space for inducing the jump. Furthermore, a short ISB length cannot ensure acceptable performance with regard to energy dissipation in cases of extreme floods. Finally, the area located within the green dotted line in Figure 4b indicates the optimum geometry of ISBs, i.e., high dissipation of energy, a more stabilized flow, and relative cost efficiency. Using this flow pattern map, the ISB length and end-sill height were optimized.

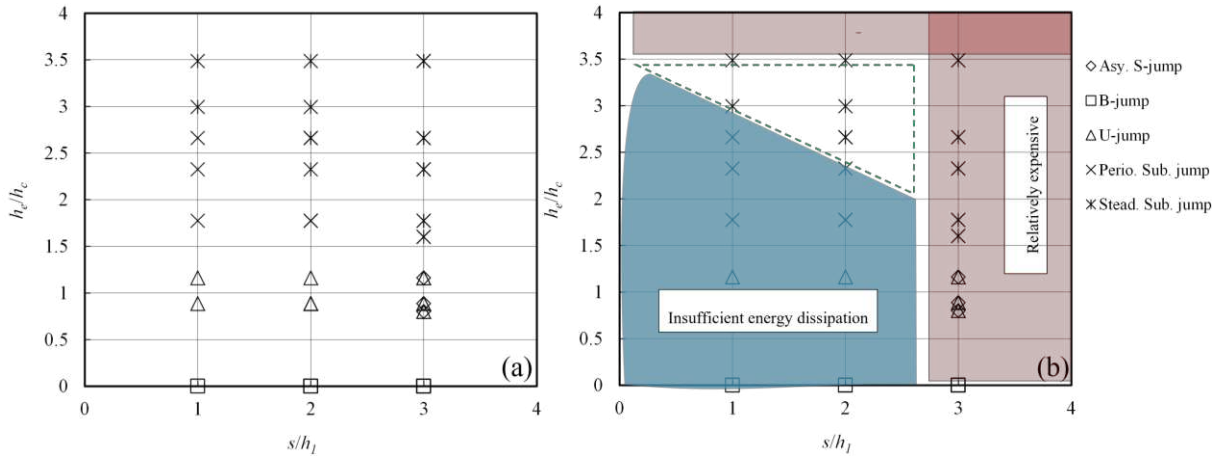


Fig. 5. (a) Flow pattern map, drop number versus normalized end-sill height. (b) Acceptable window in flow pattern map for design purposes, considering the drop number and normalized end-sill height.

Using the same data, a universal flow pattern map was presented from a different perspective. Figure 5a illustrates the relationship between drop number, s/h_1, and normalized end-sill height, h_e/h_c, for five different possible flow patterns within an ISB. Figure 5b attempts to show which area on the flow pattern map is more favorable for design purposes. The areas of the flow pattern map that are considered to be expensive geometries are colored red, and the areas where insufficient energy dissipation occurs are highlighted in blue. The area located within the green dotted lines is our expected optimum geometry. In conclusion, the flow pattern maps (Figures 3 to 5) provide a straightforward means to deduce an initial estimation of the optimum geometry of an ISB (for $2.5 < Fr < 5.5$).

3.4. Design Guideline

3.4.1. Prediction of minimum required degree of submergence

As previously introduced, Y_3, the degree of submergence, is defined as the ratio of the water depth above the lower invert of the bottom outlet to the bottom outlet opening height, h_1. Plotting the normalized ISB length versus Y_3 revealed a boundary separating the different types of jumps. This boundary provides useful information to help designers determine the minimum required degree of submergence that produces a specific type of jump. For instance, Figure 6 depicts the minimum required Y_3 for inducing a periodic submerged jump within an ISB. The red dotted line in this figure shows the boundary between a U-jump and a periodic submerged jump. The average $(h_e+s)/h_1$, which is the normalized step and end-sill height, should be greater and equal than or equal to 3.7 to provide a periodic

submerged jump independent of the normalized ISB length.

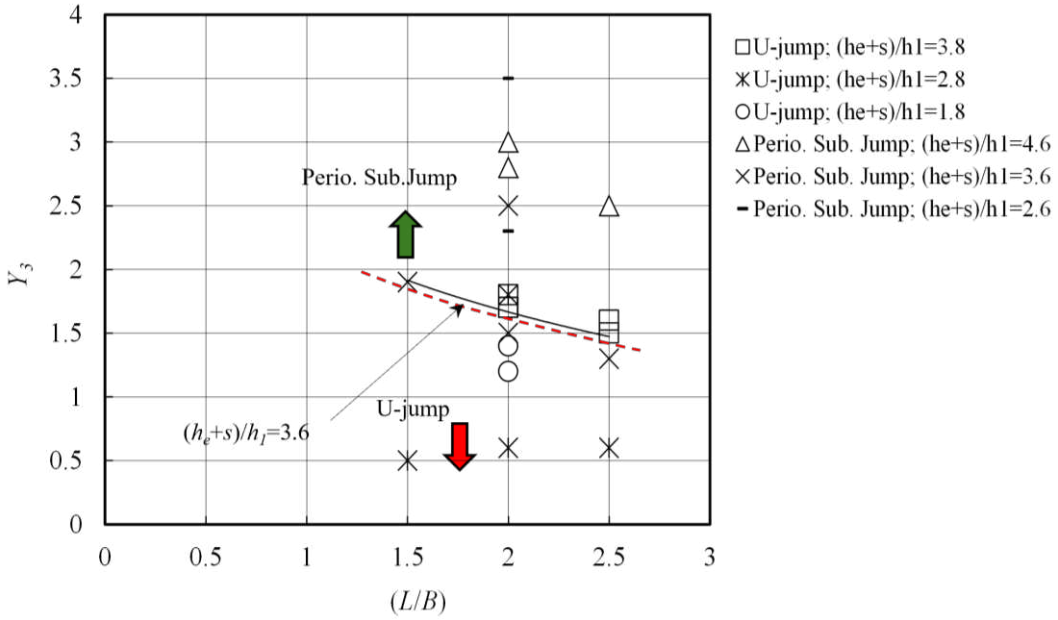


Fig. 6. Relationship between degree of submergence and normalized ISB length, the boundary between U-jump and Perio. Sub. Jump.

Figure 7 illustrates the $(h_e+s)/h_1$ that could provide the minimum required Y_3 needed for forming the periodic submerged hydraulic jump within an ISB. The minimum required submergence depth can be calculated using the following equation:

$$Y_3 = 0.0015\left(\frac{s+h_e}{h1}\right)^{4.6} \quad (4)$$

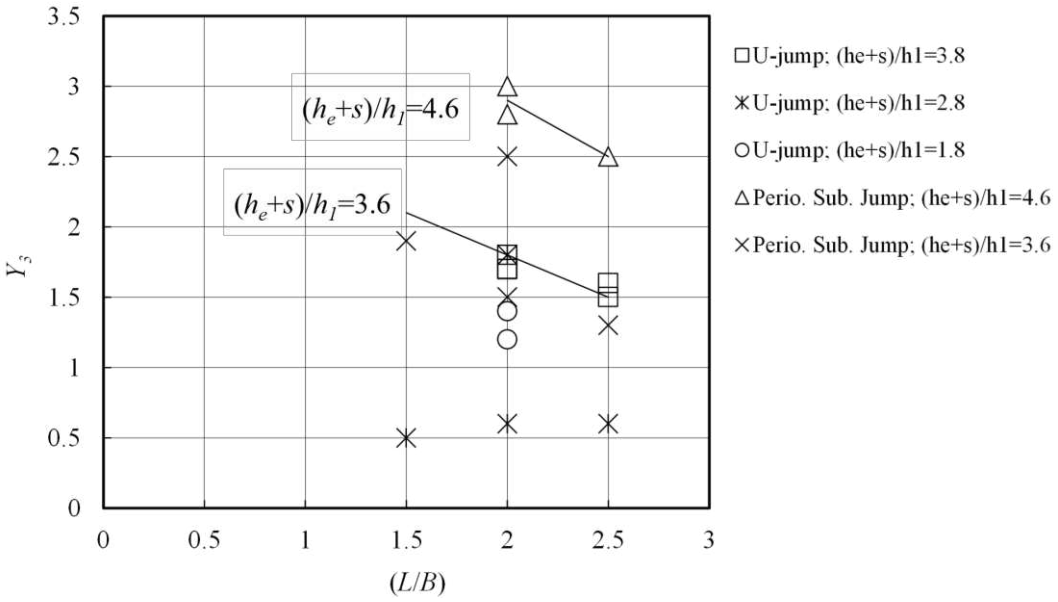


Fig. 7. The relationship between submergence depth and normalized ISB length for different normalized

299 step and end-sill height in the presence of periodic submerged jumps.

300 ***3.4.2. Prediction of the ISB length***

301 The proper estimation for the ISB length (L_B), or in other words, the end-sill location from the bottom
302 outlet, is crucial. If the end-sill is placed too close to the bottom outlet, the jump would not have
303 sufficient space to be induced. On the other hand, a very long ISB length is not cost-efficient. In fact,
304 the location of the end-sill should be balanced between ensuring sufficient energy dissipation and logical
305 costs (Larson, 2004).

306 Accurately estimating ISB length has remained a persistent challenge for hydraulic designers due to
307 the complexities involved in characterizing forced submerged jumps. So far, various definitions of ISB
308 length have been proposed. For instance, Rajratnam and Subramanya (1968) believed that the section
309 downstream of the jump where the flow velocity distribution is uniform should be considered as the end
310 of the jump, or in other words, the stilling basin length. This definition, however, leads to a very
311 expensive design for the structure, and it is not favorable. Bremen and Hager (1993) defined the length
312 of the jump to be where no more air bubbles are visible on the surface of water downstream of the jump.
313 However, this definition may work for only certain types of jumps, including B-jumps, S-jumps, and U-
314 jumps, but it may not be suitable for a submerged hydraulic jump. Ohtsu et al. (1999) followed another
315 idea for the detection of the basin length. They considered the section where rollers ceased to exist as
316 the length of submerged hydraulic jumps below a sudden lateral enlargement. In the present research,
317 the definition of Ohtsu et al. (1999) has also been followed to detect the submerged jump length. Zare
318 (2007) considered the length of scouring within a stilling basin as the length of the submerged jump.
319 However, this introduces uncertainties, such as the dependence of scour length on sediment particle
320 diameter. The question then becomes which particle size can provide a more accurate estimation of the
321 submerged jump length. Moreover, in the case of fine particles, almost all the sediment particles are
322 flushed out from the stilling basin, and almost the whole length of the stilling basin is clean of sediment.
323 To minimize these uncertainties, the definition provided by Ohtsu et al. (1999) was adopted to describe
324 the length of submerged hydraulic jumps. Therefore, to determine the length of forced hydraulic jumps
325 with an end-sill, it has been proposed by Forester and Skrinde (1950) that the ISB length (L_B) should be
326 equal to five times the sequent depth, h_2.

$$L_B = 5 \times h_2 \quad (5)$$

They also proposed an empirical equation to obtain the required height of the end-sill, h_e to create accomplished jumps upstream of the end-sill as follows:

$$h_e = h_1(0.0331 \times Fr_1^2 + 0.4385Fr_1 - 0.6534) \quad (6)$$

where h_1 and Fr_1 are the upstream approach flow depth and the Froude number, respectively. However, Larson (2004) recommended that to satisfy a conservative design and be prepared for unexpected flow discharges, it is better to use the sequent depth of classical hydraulic jumps, h_2^* instead of the sequent depth of forced hydraulic jumps proposed by Forester and Skrinde (1950) to calculate the length of the stilling basin.

$$L_B = 5 \times h_2^* \quad (7)$$

The sequent depth of classical hydraulic jumps is denoted as h_2^* and can be calculated using Belanger's (1828) famous equation:

$$\frac{h_2^*}{h_1} = \frac{1}{2}\left(\sqrt{1 + 8F_1^2} - 1\right) \quad (8)$$

Both equations provided by Forester and Skrinde (1950) and Larson (2004) are not directly devoted to submerged hydraulic jumps. Moreover, the calculation of the stilling basin length in their proposed methods leads to a very long stilling basin length.

Ohtsu et al. (2000) proposed a series of equations to obtain the length of a submerged hydraulic jump (L_{sj}). They believe that the length of a submerged jump (L_{sj}) can be considered equivalent to the length of the stilling basin ($L_{sj} = L_B$). However, they recommended considering a 1.05 – 1.15 safety factor on the ISB length. For the steady submerged hydraulic jumps, they proposed the following equation to calculate the length of the submerged jump:

$$log_{10}\left(\frac{L_{sj}}{H_L}\right) = -1.71\left(\frac{H_L}{H_1}\right) + 1.79 \quad \text{for } 0.25 \leq \frac{H_L}{H_1} \leq 0.75 \quad (9)$$

where HL is the head loss due to the submerged hydraulic jumps and H_1 is the total energy head at the bottom outlet cross section (section *1*), which can be defined as:

$$\frac{H_L}{H_1} = \frac{2(Y_3 - Y_2) + \left\{1 - \left(\frac{k}{Y_2}\right)^2\right\}}{2Y_3 + F_1^2} \quad (10)$$

where $Y_2 = h_2/h_1$, and $Y_3 = h_3/h_1$ in which h_1 is the bottom outlet opening height, h_2 is the sequent

depth, h_3 is the submergence depth at the face of the bottom outlet, and k is the expansion ratio, b_1/B. Equation (10) is one of the most reliable equations that exists in the literature concerning steady submerged hydraulic jumps below a sudden lateral enlargement; having said that, in their study, they did not consider an abrupt drop (negative step). Also, the type of submerged jumps that were studied in Ohtsu et al. (2002) were not forced hydraulic jumps by an end sill. These differences between their study and this study may limit the applicability of their equations to these design guidelines. This constraint motivated us to provide a new updated equation suitable for our case study to accurately estimate the ISB length.

Zarre (2007) claimed that the length of scouring within a stilling basin is equivalent to the length of the stilling basin. They noticed that the value of the length of the submerged jump obtained through their definition is consistent with the definition provided by Ohtsu et al. (1999). Equation (11) is proposed by Zare (2007). In his study, the submerged jumps were forced by a sill below a sudden lateral enlargement.

$$log_{10}\left(\frac{L_B}{H_L}\right) = -1.71\left(\frac{H_L}{H_1}\right) + 1.58 \quad (11)$$

By following the Ohtsu et al. (1999) definition for stilling basin length, at the end of the roller in a submerged hydraulic jump, the length of the jump is measured. Notably, in an ISB, the presence of an end sill results in a roller length only slightly shorter than the stilling basin length. Figure 8a depicts the fitted curve to the experimental data obtained in the current study describing the relationship between energy dissipation and ISB length. Moreover, the proposed fitted curve related to the current study is compared with those equations proposed by Ohtsu et al. (1999) and Zare (2007). The overall trend of all three studies seems to be quite similar. However, the ISB length in our study is slightly shorter than in previous studies and arises from the presence of both drop depth and end-sill height, which forces the jump to be as confined as possible. The trendline based on the present research is shown by the green dotted line in Figure 8a. The fitted relationship is presented in Equation (12) and can be used to estimate the ISB length:

$$log_{10}\left(\frac{L_B}{H_L}\right) = -1.65\left(\frac{H_L}{H_1}\right) + 1.4 \quad (12)$$

To estimate the normalized energy dissipation within an ISB, also, a three-dimensional theoretical equation is also proposed (Equation 13) that includes all the important geometric variables e.g. drop number, normalized ISB length, expansion ratio, sequent depth and degree of submergence. Equation (14) shows equation (13) in dimensional form.

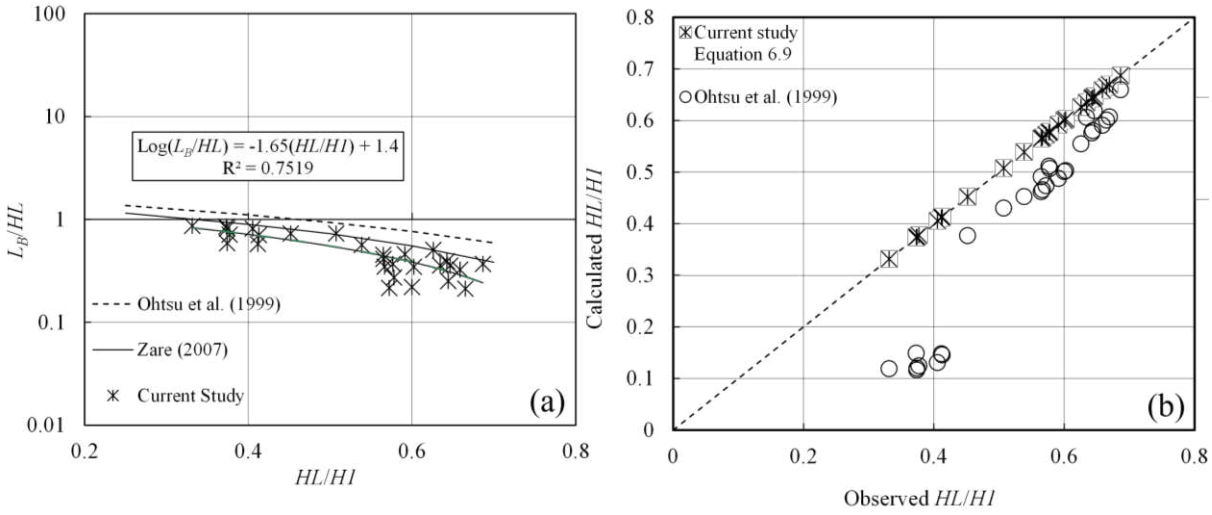


Fig. 8. (a) Relationship between normalized energy dissipation and normalized ISB length. (b) Validation of Equation 14 in the prediction of energy dissipation within ISB.

$$\frac{H_L}{H_1} = \frac{Fr_1{}^2\left(1-(k/Y_2)^2\right)+2(Y_3-Y_2)+2S}{Fr_1{}^2+2Y_3+2S} \quad (13)$$

$$\frac{H_L}{H_1} = \frac{\left(\frac{U_1{}^2}{2g}+h_3+s\right)-\left(\frac{\overline{U_2}^2}{2g}+h_2\right)}{\frac{U_1{}^2}{2g}+h_3+s} \quad (14)$$

where H_L is the head loss due to the submerged jump, H_1 is the total head at the bottom outlet face, U_1 is the initial bottom outlet velocity, h_3 is the submergence depth at the face of the drop, $\overline{U_2}$ and h_2 are, respectively, the average velocity and average water depth upstream from the end-sill. The value obtained by Equation 14 should be used as an input in Equation 13 to determine the ISB length.

Ohtsu et al. (1999) also proposed a non-dimensional form of the energy equation in which they did not consider the drop number (Equation 14). However, Figure 8 shows evidence of the importance of the drop number in the calculation of energy dissipation. Using Equation 14 from Ohtsu et al. (1999) underestimates energy dissipation. This discrepancy may further be due to the presence of the end-sill and the forcing of the hydraulic jump within the ISB.

$$\frac{H_L}{H_1} = \frac{Fr_1{}^2\left(1-(k/Y_2)^2\right)+2(Y_3-Y_2)}{Fr_1{}^2+2Y_3} \quad (15)$$

3.4.3. Prediction of normalized sequent depth

To calculate the sequent depth, h_2, for the forced submerged hydraulic jump, the momentum equation was applied, neglecting the bed shear stress between sections *I* and *II*.

$$\frac{1}{2}\gamma B{h_3}^2 + \gamma Bs\left(h_3 + \frac{s}{2}\right) - \frac{1}{2}\gamma B{h_2}^2 = \rho Q(\overline{U_2} - U_1) \quad (16)$$

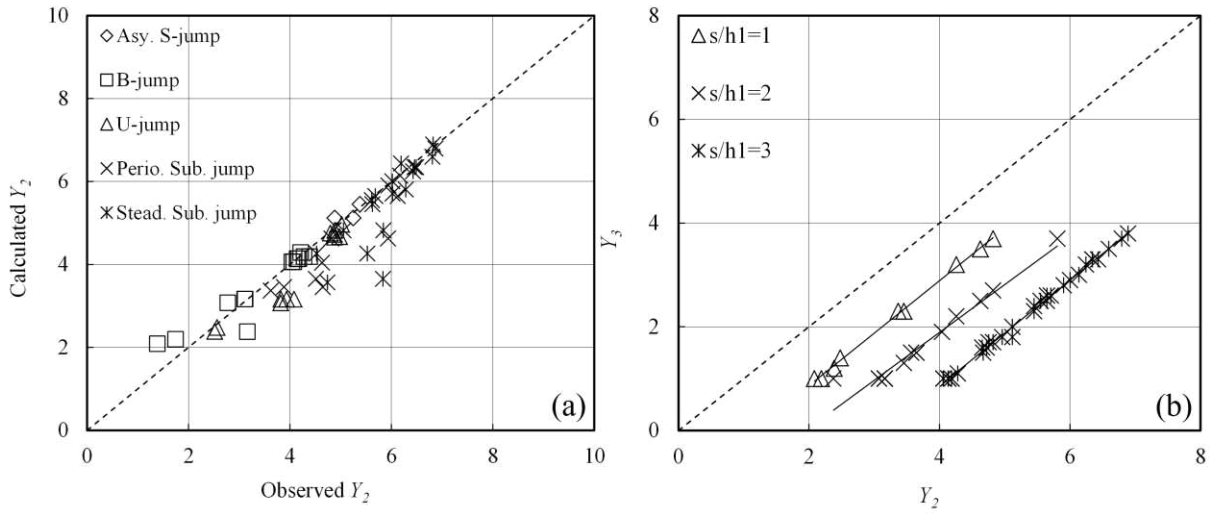
where h_3 is the submergence depth at the face of the bottom outlet, h_2 is the sequent depth upstream from the end-sill, $\overline{U_2}$ is the average velocity at section *II* is equal to the ratio of discharge Q and wetted area ($h_2 \times B$) in section *II*, ρ is the density of water, and γ is the specific weight of water. After substitution of the non-dimensional parameters in Equation 16, followed by simplification, the preceding equation can be expressed as:

$${Y_2}^3 - \left({Y_3}^2 + 2Y_3S + S^2 + 2{Fr_1}^2k\right)Y_2 + 2{Fr_1}^2k^2 = 0 \quad (17)$$

where Y_2 is the normalized sequent depth, $Y_2 = h_2/h_1$, S is the drop number, $S = s/h_1$, and k is the expansion ratio, $k = b_1/B$. Figure 9 shows the comparison between the predicted and measured relative sequent depth using Equation 17. As can be seen, Equation 17 provides an amenable prediction of measured relative sequent depth, not only for submerged hydraulic jumps but also for other possible flow patterns within an ISB. Notably, submerged hydraulic jumps within an ISB are significantly influenced by turbulence from the end-sill and characterized by reverse flow. Thus, predicting sequent depth in this case encounters a real challenge.

3.4.4. Prediction of drop depth

By applying Equation 17 to the experimental data obtained in the present research, Y_2 was calculated. Figure 9a shows the relationship between the calculated Y_2 and the observed degree of submergence, Y_3. Three linear trends are evident in this graph. Each trend represents a drop number, $S = s/h_1$, studied in this research. This figure can be used for selecting the suitable drop number when either the relative sequent depth Y_2, or the degree of submergence Y_3 is known. This figure also confirms the importance of the drop number, *S*, and its influence on other hydraulic parameters.

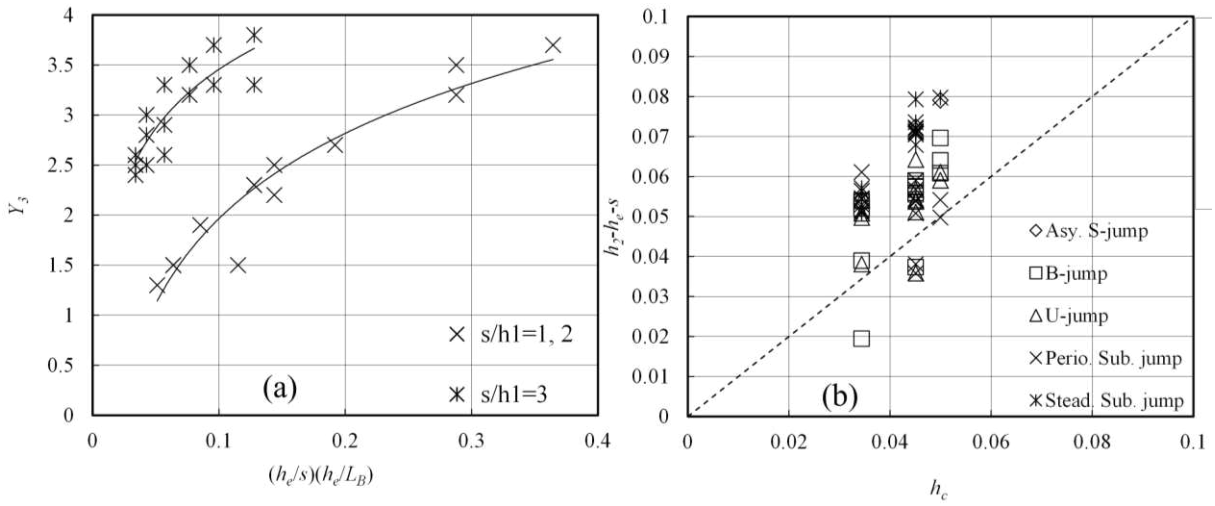


423

424 **Fig. 9**. (a) The comparison between the predicted Y_2 using Equation 17 and the observed relative sequent
425 depth. (b) The relationship between calculated Y_2 using Equation 17 and the observed degree of
426 submergence, Y_3.

427 ***3.4.5. Prediction of relative end-sill height***

428 Figure 10a provides the relationship between the degree of submergence, Y_3, within an ISB and a
429 non-dimensional parameter consisting of ISB length, depth, and end-sill height. By knowing the ISB
430 length, drop depth (step height), and degree of submergence from preceding sections, the end-sill height
431 can be selected. To adequately design the end-sill height, it is highly essential to consider, not only the
432 flow characteristics and ISB performance but also the downstream flow conditions. The energy equation
433 between the end-sill section and the downstream section can be estimated using Equation (18).



434

435 **Fig. 10**. (a) Relationship between degree of submergence within ISB and a normalized multiple

combination of ISB length, depth and end-sill height. (b) Critical depth, h_c, versus the water column above the end-sill h_2 - (h_e + s).

$$h_2 + \frac{(\frac{Q}{B(h_2-(h_e+s))})^2}{2g} = h_4 + s + \frac{(\frac{Q}{Bh_4})^2}{2g} \quad (18)$$

where $h_2 - (h_e + s)$ is the water column above the end-sill, B is the width of the channel, h_4 is the water depth downstream of the ISB (section *IV*), Q is the design discharge, and g is the gravitational acceleration. To facilitate the procedure of design for the end-sill, the critical depth, h_c, may be used instead of $h_2 - (h_e + s)$ in Equation 18. Figure 10a investigates the feasibility of the relationship between h_c and $h_2 - (h_e + s)$ for the experimental data of the present study. As can be seen, the water column above the end-sill is usually greater than the critical depth, h_c. Thus, these two values are not identical, particularly for submerged hydraulic jumps. But the more important question is whether the water level at section *IV* is calculated using the energy equation with $h_2 - (h_e + s)$ differs significantly from the calculation using h_c. Figure 10b investigates this question. This figure reveals that, whether using $h_2 - (h_e + s)$ or h_c, there is no significant difference in the accuracy of the calculated h_4. Thus, it is sufficient to use h_c in place of $h_2 - (h_e + s)$ for greater ease in design. Therefore, assuming there is a critical depth, h_c, above the end-sill, and assuming the energy loss for free fall over the end-sill is negligible, a simple energy equation between the end-sill section and section *IV* can be written as below:

$$h_c + h_e + \frac{(\frac{Q}{Bh_c})^2}{2g} = h_4{}' + \frac{(\frac{Q}{Bh_4})^2}{2g} \quad (19)$$

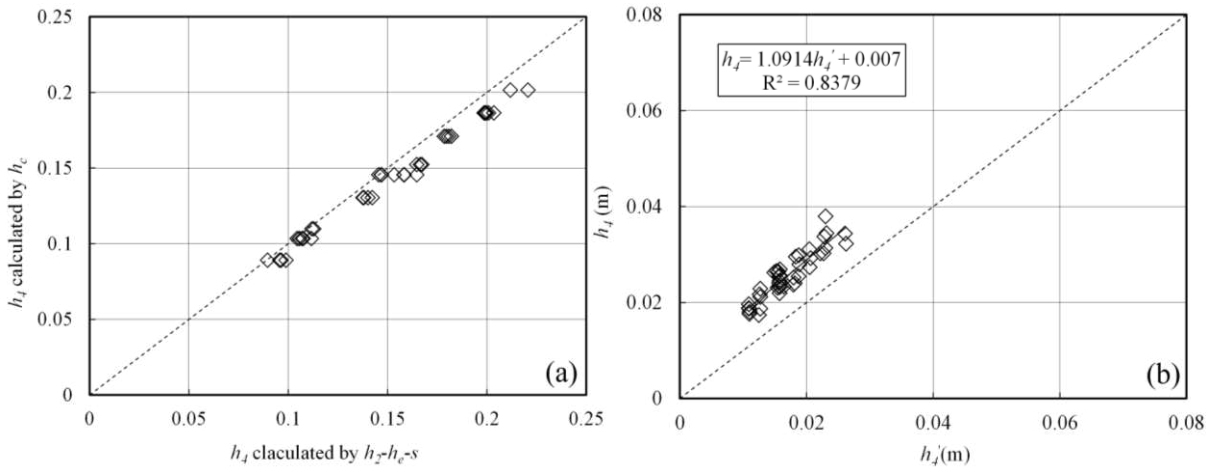


Fig. 11. (a) Investigating the accuracy of using h_c as the water column above the end-sill to compute the h_4 downstream of the ISB. (b) The gap between the calculated water depths ($h_4{}'$) at section *IV* with the

measured values.

However, in reality, the energy loss by free fall over the end-sill is not negligible (Larson, 2004) and it varies depending on the end-sill height, h_e. The comparison between the measured values of h_4 at section *IV*, and the results obtained by the theoretical method (Equation 19) demonstrates the existence of considerable energy loss over the end-sill (Figure 11a). Therefore, empirical equations were proposed to map h_4', assuming no energy loss over the end-sill to the measured values of h_4.

Equation 20 can be used to modify the calculated water depth by Equation 19 at section *IV*, in the design procedure.

$$h_4 = 1.094h_4' + 0.007 \quad (20)$$

The end-sill height is obtained using Figure 11b, by selecting the desired Froude number (Fr_4) at section *IV*, and finding the corresponding h_e/h_4 value on the vertical axis. Section *IV* is located at a distance *B* (= 50 cm) downstream of the ISB. By knowing the h_4, the width of the channel, B, as well as the design discharge, *Q*, all the necessary parameters to determine the boundary condition downstream of the end-sill are complete.

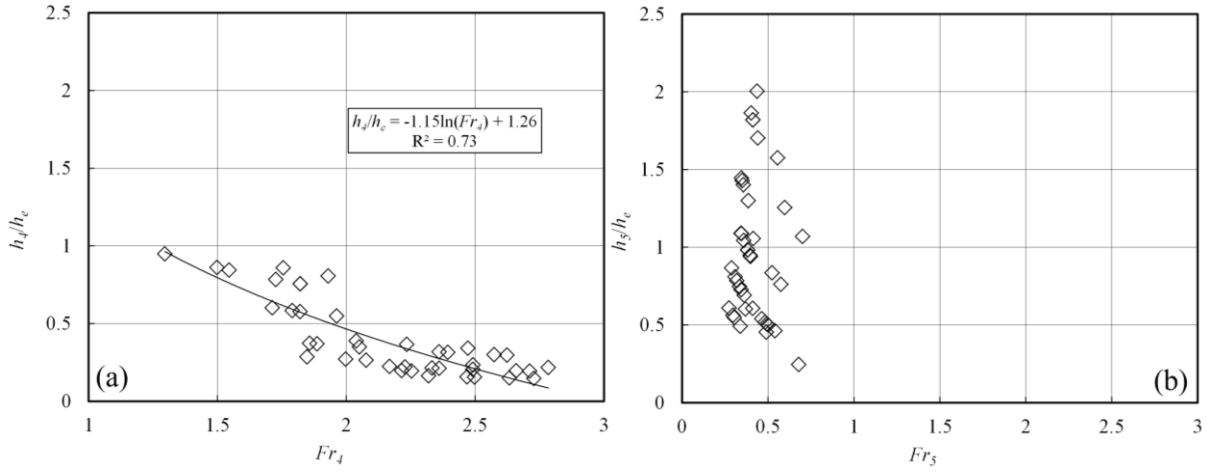


Fig. 12. (a) Froude number at section *IV* versus the normalized ratio of water depth at section *IV* over end-sill height. (b) Froude number at section *V* versus the normalized ratio of water depth at section *V* over end-sill height, h_5/h_e.

However, the water depth and average velocity in a section further down from the ISB section *V*, were also measured. Section *V* is located 4B (= 200 cm) downstream of the ISB. In this section, the flow condition is subcritical. The relationship between Fr_5 and h_5/h_e is shown in Figure 12b.

3.5. Design Procedure

Figure 13 presents a comprehensive, engineer-oriented flowchart for the complete design procedure of ISBs. It systematically illustrates the sequential steps (from input parameters Q, h_1, b_1 to the final downstream Froude number check), initial trial assumptions (S = 2, Y_2 = 4), key calculations (submergence degree, ISB length, end-sill height), verification conditions (SSJ formation and $Fr_4 \leq 0.5$), and iteration loops if the criteria are not met.

Each step is directly linked to its relevant Equations (e.g., Eqs. 14, 17) and Figures (e.g., Figs. 8a, 9b, 10a, 12a), allowing for a rapid, reliable, and practical design process. This structured framework enables construction design engineers to quickly identify controlling hydraulic parameters and optimize structural dimensions under varying flow conditions. It also provides a clear reference for integrating field observations and numerical simulations, ensuring that the ISB design meets both theoretical and site-specific performance requirements.

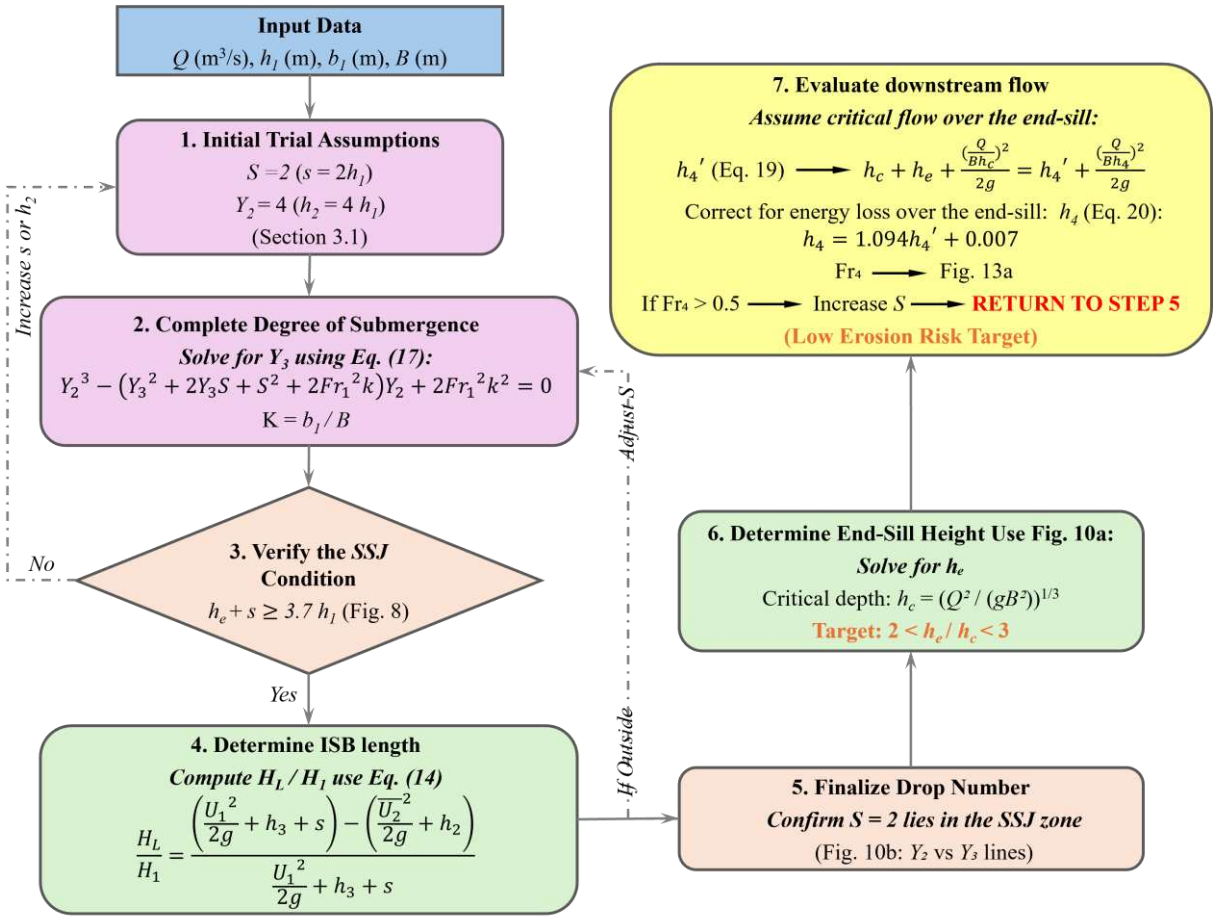


Fig. 13. Design Procedure for In-Ground Stilling Basins.

4. Discussion

The present findings highlight the critical role of geometric configuration in controlling flow patterns, hydraulic jump stability, and energy dissipation within in-ground stilling basins (ISBs). The experimental results indicate that the combined effects of abrupt drops, sudden expansions, and end-sills substantially influence the hydraulic performance of ISBs. In particular, the formation of steady submerged jumps (SSJs) represents a favorable hydraulic condition because of their relatively stable and symmetric flow structure and effective velocity reduction. Although periodic submerged jumps can also produce considerable velocity reduction, their unsteady characteristics may introduce undesirable fluctuations within the basin. These observations emphasize that hydraulic efficiency should be evaluated not only in terms of energy dissipation but also with respect to flow stability and downstream hydraulic conditions.

The results further demonstrate that the relative end-sill height, basin length, and drop number are important parameters governing hydraulic jump characteristics. Increasing the end-sill height promotes flow submergence and facilitates the transition toward submerged hydraulic jumps. However, excessively high end-sills may increase construction requirements without providing proportional hydraulic benefits. Similarly, increasing the basin length does not necessarily improve hydraulic performance, highlighting the importance of selecting appropriate geometric proportions rather than simply enlarging the structure. Within the investigated experimental conditions, the recommended geometric ranges provide a practical balance between hydraulic performance and structural dimensions.

Compared with previous investigations focusing primarily on individual geometric modifications, the present study considers their combined influence on flow behavior and energy dissipation. The proposed analytical and empirical relationships incorporate key geometric and hydraulic parameters, providing a more integrated approach to predicting energy losses and sequent depths. The agreement between predicted and measured values supports the applicability of these relationships within the investigated conditions. Nevertheless, their predictive capability beyond the tested geometric configurations and hydraulic ranges requires further validation.

From an engineering perspective, the proposed design procedure provides a systematic framework for selecting ISB dimensions while considering both internal flow characteristics and downstream hydraulic requirements. The integration of flow pattern identification, geometric selection, and downstream Froude number assessment offers a practical approach to improving energy dissipation and flow stability. These findings contribute to the hydraulic design of stilling basins downstream of flood mitigation dams, where effective energy dissipation and controlled downstream flow conditions are essential for maintaining structural safety. The present findings highlight the critical role of geometric configuration in controlling flow patterns, hydraulic jump stability, and energy dissipation within in-ground stilling basins (ISBs). The experimental results indicate that the combined effects of abrupt drops, sudden expansions, and end-sills substantially influence the hydraulic performance of

ISBs. In particular, the formation of steady submerged jumps (SSJs) represents a favorable hydraulic condition because of their relatively stable and symmetric flow structure and effective velocity reduction. Although periodic submerged jumps can also produce considerable velocity reduction, their unsteady characteristics may introduce undesirable fluctuations within the basin. These observations emphasize that hydraulic efficiency should be evaluated not only in terms of energy dissipation but also with respect to flow stability and downstream hydraulic conditions.

The results further demonstrate that the relative end-sill height, basin length, and drop number are important parameters governing hydraulic jump characteristics. Increasing the end-sill height promotes flow submergence and facilitates the transition toward submerged hydraulic jumps. However, excessively high end-sills may increase construction requirements without providing proportional hydraulic benefits. Similarly, increasing the basin length does not necessarily improve hydraulic performance, highlighting the importance of selecting appropriate geometric proportions rather than simply enlarging the structure. Within the investigated experimental conditions, the recommended geometric ranges provide a practical balance between hydraulic performance and structural dimensions.

Compared with previous investigations focusing primarily on individual geometric modifications, the present study considers their combined influence on flow behavior and energy dissipation. The proposed analytical and empirical relationships incorporate key geometric and hydraulic parameters, providing a more integrated approach to predicting energy losses and sequent depths. The agreement between predicted and measured values supports the applicability of these relationships within the investigated conditions. Nevertheless, their predictive capability beyond the tested geometric configurations and hydraulic ranges requires further validation.

From an engineering perspective, the proposed design procedure provides a systematic framework for selecting ISB dimensions while considering both internal flow characteristics and downstream hydraulic requirements. The integration of flow pattern identification, geometric selection, and downstream Froude number assessment offers a practical approach to improving energy dissipation and flow stability. These findings contribute to the hydraulic design of stilling basins downstream of flood mitigation dams, where effective energy dissipation and controlled downstream flow conditions are essential for maintaining structural safety.

5. CONCLUSION AND FUTURE DIRECTIONS

This experimental study provides an in-depth analysis of flow behavior in In-Ground Stilling Basins (ISBs), focusing on classifying hydraulic jumps and optimizing ISB geometry to enhance energy dissipation. By evaluating the influence of geometric parameters and hydraulic conditions on flow patterns, the following conclusions are drawn:

- The principal jump regimes discussed in the design assessment include B-jumps (BJ), U-jumps

(UJ), periodic submerged jumps (PSJ), and steady submerged jumps (SSJ). The steady submerged hydraulic jump (SSJ) was determined to be the most effective in terms of velocity reduction, flow stability, and symmetry, making it a preferred option for energy dissipation in ISB designs.

- The inverse ratio of cross-wall height to ISB length emerged as a critical parameter distinguishing periodic submerged jumps (PSJ) from steady submerged jumps (SSJ). Flow patterns within the ISB were found to be more dependent on cross-wall height than on upstream hydraulic conditions, such as the Froude number. However, increasing the ISB length was observed to reduce flow stability, underscoring the importance of optimizing this geometric parameter.
- Based on the experimental findings, various flow patterns were observed to depend on ISB geometry, affecting performance. Identifying the relevant flow pattern and proposing a corresponding design guideline are essential. Therefore, this study provides a step-by-step design procedure for ISB downstream.
- A series of empirical and theoretical equations for predicting energy loss and sequent depth were developed by solving the momentum and continuity equations. These equations demonstrated high consistency with experimental data, confirming their applicability for the complex geometry of ISBs and providing a reliable tool for design optimization.

Future studies are recommended to extend this analytical framework to cover additional ranges of Froude numbers and diverse ISB configurations, including alternative cross-sectional shapes and sediment transport processes. Additionally, it is essential for subsequent research to undertake field validations of the proposed empirical adjustments for cross-wall height under actual flood scenarios to strengthen the applicability and reliability of the developed model. Finally, this study establishes a robust foundation for the continued refinement of ISB design practices, thereby contributing to enhanced resilience and sustainability in flood mitigation infrastructure.

Notation

b_1 = The bottom outlet opening width (m)

B = In-ground stilling basin (ISB) width (m)

590 B_r = Downstream river width (m)

591 F_1 = Froude number at the face of the bottom outlet (-)

592 F_4 = Froude number at section *IV* (-)

593 g = the gravitational acceleration (ms^2)

594 h_1 = The bottom outlet opening height (m)

595 h_e = Cross wall height (m)

596 h_c = Critical depth (m)

597 $k = b_1/B$ = The expansion ratio (-)

598 L = In-ground stilling basin (ISB) length (m)

599 R = Reynolds number (-)

600 Q = Flow discharge (m^3/s)

601 Q = Discharge per unit width (m^2s^{-1})

602 s = The drop depth (step height) (m)

603 $S = s/h_1$ = Drop number (-)

604 U_0 = Initial velocity at the face of the bottom outlet (m/s)

605 U_2 = Maximum mean velocity at section *II* (m/s)

606 W = Weber number (-)

607 $Y_2 = h_2/h_1$ = The normalized sequent depth (-)

608 $Y_3 = h_3/h_1$ = The normalized submergence depth (-)

609 ρ = The water density

610 σ = The surface tension (-)

611 μ = the dynamic viscosity

612

613 **Data Availability Statement**

614 Data that support the findings of this study are available from the corresponding author upon

615 reasonable request.

616

Acknowledgement

[Blinded]

Conflict of Interest

The authors declare that there is no conflict of interest regarding the publication of this paper.

Author Contributions

[Blinded]

REFERENCES

Akan, O.B. Karli, O. Ergul,. (2009). Cognitive Radio Sensor Networks, IEEE Network 23 (4)34–40. https://doi.org/10.1109/MNET.2009.5191144

Anzani, H., Kantoush, S.A., Mahdian Khalili, A. and Hamidi, M., (2025a). Experimental and analytical investigation of energy loss in low-discharge weirs with rectangular opening. Modeling Earth Systems and Environment, 11(6), p.418. https://doi.org/10.1007/s40808-025-02620-8

Anzani, H., Ghodsian, M. and Kantoush, S.A., (2025b). Energy loss prediction and analysis for rectangular, triangular, and trapezoidal piano key weirs. AQUA-Water Infrastructure, Ecosystems and Society, p.jws2025034.

Bremen, R. (1990). Expanding stilling basin (No. BOOK). EPFL-LCH.

Bremen, R., and Hager, W. H. (1994). Expanding stilling basin. Proc., ICE Water Maritime Engineering, 106 (3), 215–228.

Chow, V. T. 1959. Open Channel Hydraulics. McGraw-Hill. New York.

Ferreri, G.B., and Nasello, C. (2002), Hydraulic jumps at drop and abrupt enlargement in rectangular channel, Journal of hydraulic research, Vol.40, No.4, pp.491-504. https://doi.org/10.1080/00221680209499891

Hager, W. H., and Li, D. (1992). Sill-controlled energy dissipater. Journal of Hydraulic Research, 30(2), 165-181. https://doi.org/10.1080/00221689209498932

Heller, V. (2011). Scale effects in physical hydraulic engineering models. Journal of Hydraulic Research, 49(3), 293-306. https://doi.org/10.1080/00221686.2011.578914

645 Katakam V.S.R., Rama P. (1998). Spatial B-jump at sudden channel enlargements with abrupt drop.
646 Journal of hydraulic engineering, Vol.124, No.6, pp.643-646.
647 https://doi.org/10.1061/(ASCE)0733-9429(1998)124:6(643)
648 Kantoush, S. A., and Sumi, T., (2010). Influence of stilling basin geometry on flow pattern and sediment
649 transport at flood mitigation dams, 9th FISC, The Federal Interagency Sedimentation Conferences,
650 Las Vegas, Nevada, pp. 115-133.
651 Kiani, S., Fathimoghadam, M., Behroozirad, R., and Davoodi, L. (2017). Control of hydraulic jump in
652 the stilling basins with perforated sill. Irrigation and Water Engineering, 7(4), 26-36.
653 Larson E. A. (2004), Energy dissipation in culverts by forcing a hydraulic jump at the outlet, Thesis on
654 Master of Science in civil engineering, Washington state University.
655 Mahtabi, G., Chaplot, B., Azamathulla, H. M., and Pal, M. (2020). Classification of 663 hydraulic jump
656 in rough beds. Water, 12(8), 2249. https://doi.org/10.3390/w12082249
657 Meshkati Shahmirzadi, M. E., Sumi, T. (2013). Hydraulic design of in-ground stilling basin under
658 submerged jump conditions for flood mitigation dams. Journal of Japan Society of Civil Engineers,
659 Ser. B1 (Hydraulic Engineering), 69(4), I_79-I_84. https://doi.org/10.2208/jscejhe.69.I_79
660 Meshkati, E., Kantoush, S.A., Sumi, T., Nguyen, B.Q. and Anzani, H.S., 2025. Experiments to classify
661 In-Ground Stilling Basins and Determine the Factors Affecting the Optimization of Flood
662 Mitigation Dams. Results in Engineering, p.104368. https://doi.org/10.1016/j.rineng.2025.104368
663 Mossa M., Petrillo A. and Chanson H. (2003), Tail water level effects on flow conditions at an abrupt
664 drop, Journal of Hydraulic Research, Vol.41, No.1, pp:39-51. Mossa, M., Petrillo, A. and Chanson,
665 H., 2003. Tailwater level effects on flow conditions at an abrupt drop. Journal of Hydraulic
666 Research, 41(1), pp.39-51.
667 Negm, A.M.,Abdel-Aal, G.M., Elfiky, M.M. And Mohamed, Y.A., (2003), Characteristics of
668 Submerged Hydraulic Jump in Radial Basin with a Vertical Drop in the Bed, AEJ, Vol. 42 (1),
669 65-76.
670 Ohtsu, I., and Yasuda, Y. (1991), Transition from supercritical to subcritical flow at an abrupt drop,
671 Journal of hydraulic research, Vol. 29, No. 3, pp. 309-328.
672 https://doi.org/10.1080/00221689109498436

673 Ohtsu, I., Yasuda, Y., and Ishikawa, M. (1999), Submerged hydraulic jumps below abrupt expansions,
674 Journal of hydraulic engineering, Vol. 125, No. 5, pp. 492-499.
675 https://doi.org/10.1061/(ASCE)0733-9429(1999)125:5(492)
676 Pagliara, S., Wave type flow at abrupt drop: flow geometry and energy loss, in Entropy and energy
677 dissipation in water resources (Springer Netherlands, 1992) 469-479. https://hal.science/hal-
678 04445744v1/file/LMFL_JFM_2023_LIU_Shuo.pdf
679 Rajaratnam, N. (1968). Hydraulic jumps on rough beds. Trans. Eng. Inst. Canada, 11(A-2), 1-8.
680 Sangsefidi, Y., Tavakol-Davani, H., Ghodsian, M., Mehraein, M., Zarei, R., Hydrodynamics and free-
681 flow characteristics of piano key weirs with different plan shapes, Water 13(15) (2021) 2108.
682 https://doi.org/10.3390/w13152108
683 Sohrabzadeh, H., Ghodsian, M., Experimental study of flow over piano key weirs with different plan
684 shapes, ISH Journal of Hydraulic Engineering 30(2) (2024) 185-195.
685 http://dx.doi.org/10.1080/09715010.2024.2302808
686 Sohrabzadeh, H., Kantoush, S. A., Mahdian Khalili, A., Hamidi, M., Energy Dissipation Assessment in
687 Flow Downstream of Rectangular Sharp-Crested Weirs, Water 16(23) (2024a) 3371.
688 https://doi.org/10.3390/w16233371
689 Sohrabzadeh, H., Kantoush, S. A., Mahdian Khalili, A., Hamidi, M., Experimental investigation of slit
690 weir discharge, ISH Journal of Hydraulic Engineering 30(5) (2024b) 645-654.
691 http://dx.doi.org/10.1080/09715010.2024.2401845
692 Sohrabzadeh, H. and Ghodsian, M., 2023. Energy dissipation of rectangular and trapezoidal piano key
693 weir. Irrigation and Drainage Structures Engineering Research, 24(90), pp.17-32.
694 https://doi.org/10.22092/idser.2023.362286.1545
695 Zare H. K. and Doering J. C. (2011), Forced hydraulic jumps below abrupt expansions, Journal of
696 hydraulic engineering, Vol. 137, No. 8, pp. 825-835. https://doi.org/10.1061/(ASCE)HY.1943-
697 7900.0000369